Depolarization effects from nanoimprinted grating structures as measured by Mueller matrix polarimetry

Xiuguo Chen,[1,a)] Chuanwei Zhang,[2,a)] and Shiyuan Liu[1,2,b)]
[1]*Wuhan National Laboratory for Optoelectronics, Huazhong University of Science and Technology, Wuhan 430074, China*
[2]*State Key Laboratory of Digital Manufacturing Equipment and Technology, Huazhong University of Science and Technology, Wuhan 430074, China*

(Received 4 September 2013; accepted 24 September 2013; published online 11 October 2013)

Mueller matrix polarimetry (MMP) is introduced to characterize nanoimprinted grating structures, and noticeable depolarization effects from measured data are observed. We demonstrate that these depolarization effects are mainly induced by the finite bandwidth and numerical aperture of the instrument, as well as the residual layer thickness variation of the measured sample. After incorporating the depolarization effects into the optical model, not only improved accuracy can be achieved for the line width, line height, and residual layer thickness measurement but also the residual layer thickness variation over the illumination spot can be directly determined by MMP. [http://dx.doi.org/10.1063/1.4824760]

Nanoimprint lithography (NIL),[1,2] in which features on a prepatterned mold are transferred directly into a polymer material, represents a promising technique with the potential for high resolution and throughput as well as low cost. In order to control NIL processes to achieve good fidelity, accurate characterization of structural parameters of nanoimprinted patterns is highly desirable. These parameters usually include not only the pattern height and width but also the residual layer thickness. Although both scanning electron microscopy (SEM) and atomic force microscopy (AFM) can provide high precision data, they are, in general, time-consuming, expensive, complex to operate, and problematic in realizing in-line integrated measurement. Recently, optics-based metrology techniques have been introduced to characterize imprinted nanostructures, such as specular x-ray reflectivity (SXR),[3] critical dimension small-angle x-ray scattering (CD-SAXS),[4] and ellipsometric scatterometry.[5–7] Among these techniques, scatterometry is relatively ideal due to its low cost, high throughput, and minimal sample damage.

In this work, we introduce Mueller matrix polarimetry (MMP) to characterize nanoimprinted gratings. Compared with conventional ellipsometric scatterometry, which only obtains two ellipsometric angles, MMP-based scatterometry can provide up to 16 quantities of a 4×4 Mueller matrix in each measurement. Consequently, MMP can acquire much more useful information about the sample and thereby can achieve better measurement sensitivity and accuracy.[8–10] In particular, when samples have depolarization effects, the Mueller matrix calculus is much preferred to model optical responses from depolarizing samples. We will show that MMP can be applied not only to accurately quantify line width, line height, and residual layer thickness of the nanoimprinted gratings but also to directly determine variation in the residual layer thickness over the illumination spot. The latter will result in quasi-depolarization of the incident light. While the depolarization effect induced by film thickness nonuniformity has been investigated in thin film measurements using spectroscopic ellipsometry[11,12] and the characterization of nanoimprinted gratings using MMP has also been reported,[13] the current work presents an observation of the depolarization effect induced by the residual layer thickness nonuniformity and a demonstration of the influences of depolarization effects on the characterization of nanoimprinted gratings.

A set of STU220 resist films with different thicknesses (developed by Obducat AB Co.) on (100)-orientation single crystal Si wafers were imprinted on an Eitre3 Nano Imprinter using a Si imprinting mold. The Si imprinting mold fabricated by e-beam lithography and dry etching has gratings with a pitch of 800 nm, a top critical dimension of 350 nm, a grating height of 472 nm, and a sidewall angle of 88°.[10] The cross-sectional SEM (X-SEM) (Nova NanoSEM450, FEI Co.) image of one of the nanoimprinted gratings is shown in Fig. 1. We used a dual-rotating compensator Mueller matrix polarimeter (RC2 ellipsometer, J. A. Woollam Co.) with in-house optical modeling software developed based on rigorous coupled wave analysis (RCWA)[14–16] to characterize the nanoimprinted gratings. With the dual-rotating compensator configuration, the full Mueller matrix elements can be obtained by a single measurement.[17] Figure 2 shows the Mueller matrix spectra of the nanoimprinted grating structure depicted in Fig. 1. The Mueller matrices (normalized to m_{11}) were measured at 601 points over wavelengths ranging from 200 to 800 nm in a specular mode with the incidence angle θ fixed at 65° and with the plane of incidence perpendicular to the grating lines, i.e., with the azimuthal angle φ equal to 0°. Although the azimuthal angle in the RC2 ellipsometer can be varied from 0° to 360°, we fixed it at 0° to decrease RCWA calculation time, since the RCWA calculation in a conical diffraction configuration ($\varphi \neq 0$) is much more time-consuming than in a planar diffraction configuration ($\varphi = 0$), especially when depolarization effects are incorporated into the optical model. The beam diameter in the RC2 ellipsometer can be changed from the normal value of about 3 mm to the value less than 200 μm with the focusing lens.

[a)]X. Chen and C. Zhang contributed equally to this work.
[b)]Author to whom correspondence should be addressed. Electronic mail: shyliu@mail.hust.edu.cn.

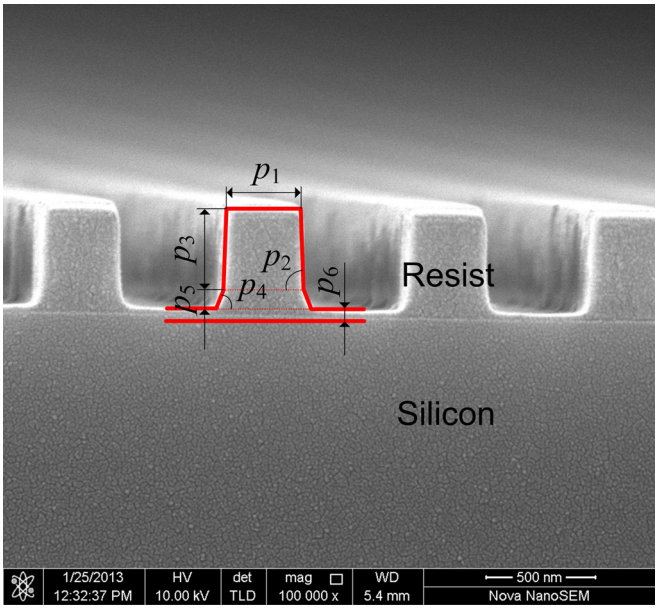

FIG. 1. X-SEM image and geometric model of the investigated nanoimprinted grating structure.

When a sample has a depolarization effect, totally polarized incident light is transformed into partially polarized light, and the associated Mueller matrix will be a depolarizing one. The depolarization effect of a depolarizing Mueller matrix can be described by the depolarization index DI that is defined by[18]

$$DI = \left[\frac{\mathrm{Tr}(\mathbf{M}\mathbf{M}^{\mathrm{T}}) - m_{11}^2}{3m_{11}^2}\right]^{1/2}, \quad 0 \le DI \le 1, \qquad (1)$$

where m_{11} is the (1, 1)th element of the Mueller matrix $\mathbf{M}$, $\mathbf{M}^{\mathrm{T}}$ is the transposed matrix of $\mathbf{M}$, and $\mathrm{Tr}(\cdot)$ represents the trace. $DI = 0$ and $DI = 1$ correspond to a totally depolarizing and non-depolarizing Mueller matrix, respectively. The depolarization index spectrum that corresponds to the polarimeter-measured Mueller matrix spectra shown in Fig. 2 is presented in Fig. 3. As can be observed from Fig. 3, the depolarization indices are close to 1 over most of the spectrum except for the range from about 300 to 460 nm and show significant dips to about 0.84 near 320 nm. Clearly, the investigated nanoimprinted grating sample exhibits noticeable depolarization effects that should be included in the interpretation of the polarimeter-measured data.

Many causes may induce depolarization effects.[19] These causes can be classified overall into two categories, namely, the extrinsic and intrinsic causes. The extrinsic causes, such as the finite bandwidth of the monochromator, the finite numerical apertures of the focusing lens in the measurement system, and the imperfect optical elements in the measurement system, will induce depolarization effects in the measurement process. The intrinsic causes include those that are closely related with the measured sample *per se* such as thickness nonuniformity, large surface or edge roughness, and thick transparent substrates. In the analysis of a depolarizing sample, we need to use an optical model that incorporates depolarization effects. The optical modeling principle is based on the optical equivalence of the polarization states,[20] which states that a depolarizing system is optically equivalent to a system composed of a parallel combination of several non-depolarizing optical systems. It can be further deduced that a depolarizing Mueller matrix can be written as the sum of various non-depolarizing Mueller matrices.

We first incorporated the depolarization effects that were induced by the finite bandwidth and numerical aperture of the RC2 ellipsometer into the optical model. According to the above-mentioned optical equivalence of the polarization states, the depolarizing Mueller matrix induced by the finite numerical aperture can be formulated as

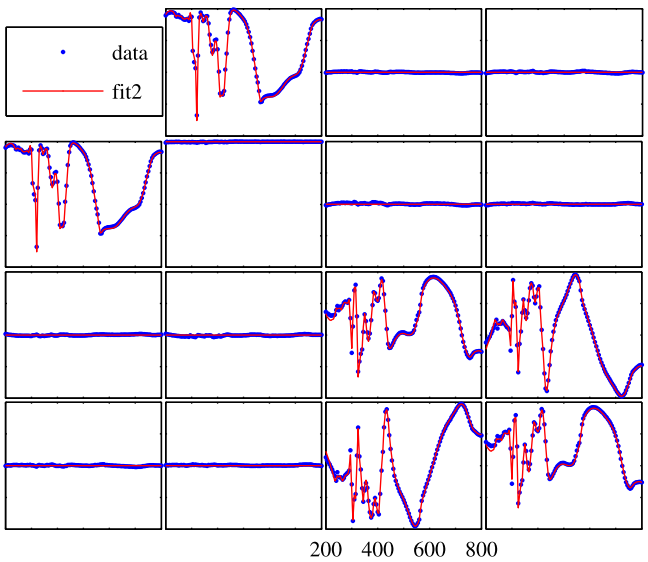

FIG. 2. Fitting result of the calculated and polarimeter-measured Mueller matrix spectra when considering the depolarization effects induced by numerical aperture, finite bandwidth, and residual layer thickness nonuniformity. The Mueller matrix elements are normalized to m_{11}, which is not shown. The horizontal axes, varying from 200 to 800 nm with an increment of 5 nm, denote the wavelengths, and the vertical axes, varying from −1 to 1, denote the values of the associated Mueller matrix elements.

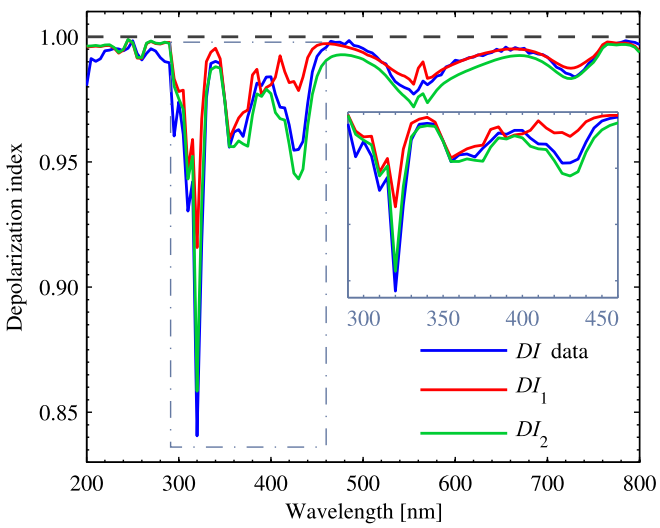

FIG. 3. Depolarization index spectra of the polarimeter-measured and calculated Mueller matrix spectra. The depolarization index spectrum DI_1 corresponds to the calculated Mueller matrix spectra when only considering the depolarization effects induced by numerical aperture and finite bandwidth. The depolarization index spectrum DI_2 corresponds to the calculated Mueller matrix spectra when considering the depolarization effects induced by numerical aperture, finite bandwidth, and residual layer thickness nonuniformity.

$$\mathbf{M} = \frac{1}{\pi r^2}\int\int_C \mathbf{M}(\theta, \varphi)d\theta d\varphi, \quad (2)$$

where C is the exit pupil with a radius of r and $\mathbf{M}(\theta, \varphi)$ is a non-depolarizing Mueller matrix corresponding to the incidence angle θ and azimuthal angle φ. Similarly, the depolarizing Mueller matrix induced by the finite bandwidth can be formulated as

$$\mathbf{M} = \int w(\lambda)\mathbf{M}(\lambda)d\lambda, \quad (3)$$

where $w(\lambda)$ is a spectral bandwidth function and $\int w(\lambda)d\lambda = 1$ and $\mathbf{M}(\lambda)$ is a non-depolarizing Mueller matrix corresponding to the wavelength λ. The calculations of Eqs. (2) and (3) require discretization of the ranges of the incidence angle θ, the azimuthal angle φ, the wavelength λ, and calculation of the non-depolarizing Mueller matrices at all specified discrete points followed by weighted averaging. The function $w(\lambda)$ can be chosen to be a Gaussian or a rectangular function.[21] The non-depolarizing Mueller matrices $\mathbf{M}(\theta, \varphi)$ and $\mathbf{M}(\lambda)$ can be directly obtained from the corresponding Jones matrices of the zeroth diffraction order,[19] which can be calculated using RCWA.

We performed nonlinear weighted least-squares fits of the measured Mueller matrix spectra $m_{ij,k}^{\text{meas}}$ to the calculated spectra $m_{ij,k}^{\text{calc}}$ using a Levenberg-Marquardt algorithm,[22] which minimizes

$$\chi_r^2 = \frac{1}{15N - P}\sum_{k=1}^{N}\sum_{i,j=1}^{4}\left[\frac{m_{ij,k}^{\text{meas}} - m_{ij,k}^{\text{calc}}}{\sigma(m_{ij,k})}\right]^2, \quad (4)$$

where k denotes the spectral point from the total number N, indices i and j show all the Mueller matrix elements except m_{11}, $\sigma(m_{ij,k})$ is the standard deviation associated with $m_{ij,k}$, and P denotes the total number of fitting parameters. In the fitting process, optical constants of the Si substrate were fixed at values taken from the literature.[23] Optical properties of the STU220 resist were modeled by using a two-term Forouhi-Bloomer model,[24] whose parameters were determined from a STU220 resist film on the Si substrate and taken as $A_1 = 0.004447$, $A_2 = 0.03051$, $B_1 = 8.8611$ eV, $B_2 = 12.0043$ eV, $C_1 = 19.6703$ eV^2, $C_2 = 36.3258$ eV^2, $n(\infty) = 1.4842$, and $E_g = 3.3724$ eV in our calculations. An accurate geometric model for the grating line profile is essential to achieve good agreement between the experimentally measured and theoretically calculated Mueller matrix spectra. As shown in Fig. 1, we applied a two-layer isosceles trapezoidal model with a total of six structural parameters $p_1 \sim p_6$ to characterize the imprinted grating line profile, where the residual layer thickness is denoted as p_6. For RCWA calculations, the number of retained orders in the truncated Fourier series is 12, and the modulated portion of the grating was divided into 25 slices.

In order to determine the bandwidth and numerical aperture of the RC2 ellipsometer, we performed a measurement on a nominally 1000 nm SiO_2 thick thermal film on a Si substrate (provided by J. A. Woollam Co.). Although the bandwidth and numerical aperture can also be determined together with the structural parameters in the following grating reconstruction process, we measured them through a SiO_2/Si standard sample so as to isolate the effects of finite bandwidth and numerical aperture from sample-specific artifacts. The measurement yielded an instrument bandwidth of $\sigma_\lambda = 1.0$ nm and a numerical aperture of $NA = 0.065$. A rectangular bandwidth function was chosen in the measurement of bandwidth. In the grating reconstruction process, we fixed the bandwidth and numerical aperture and let just the structural parameters $p_1 \sim p_6$ vary (grating pitch was fixed at the nominal value of 800 nm). The depolarization index spectrum DI_1 corresponding to the best-fit calculated Mueller matrix spectra is shown in Fig. 3. According to Fig. 3, we observe that the measured and calculated depolarization indices show good agreement within the spectral range from about 460 to 800 nm, but exhibit poor performance within the spectral range from about 300 to 460 nm. Considering that the measured depolarization index spectrum shows significant dips in the latter spectral range, it is obviously insufficient to only incorporate the depolarization effects induced by finite bandwidth and numerical aperture into the optical model.

We further took the depolarization effect induced by the residual layer thickness nonuniformity over the area of the probe light spot into account. The depolarizing Mueller matrix induced by the residual layer thickness nonuniformity can be formulated as

$$\mathbf{M} = \int \rho(t)\mathbf{M}(t)dt, \quad (5)$$

where $\rho(t)$ is a thickness distribution function and $\int \rho(t)dt = 1$. $\mathbf{M}(t)$ is a non-depolarizing Mueller matrix corresponding to the residual layer thickness t. The calculation of Eq. (5) is similar to that of Eq. (3). The function $\rho(t)$ can be chosen to be either a rectangular[11] or a Gaussian function. In the following grating reconstruction process, we still fixed the bandwidth and numerical aperture but let the structural parameters $p_1 \sim p_6$ as well as the standard deviation σ_t of the residual layer thickness vary. A Gaussian thickness distribution function was chosen in our calculation. Figure 3 depicts the comparison of the measured depolarization index spectrum with the depolarization index spectrum DI_2 that corresponds to the best-fit calculated Mueller matrix spectra. Figure 3 indicates that the agreement between the measured and calculated depolarization index spectra is significantly improved, especially in the spectral range from about 300 to 460 nm, when taking the depolarization effect induced by the residual layer thickness nonuniformity into account. It is

TABLE I. Comparison of fitting parameters extracted from the MMP and SEM measurements.

Parameter	fit1	fit2	SEM
p_1 (nm)	351.67 ± 0.146	352.29 ± 0.160	352.2
p_2 (deg)	86.80 ± 0.025	87.11 ± 0.026	87.5
p_3 (nm)	439.11 ± 1.359	442.83 ± 1.008	
p_4 (deg)	32.56 ± 2.099	25.41 ± 1.473	
p_5 (nm)	31.42 ± 1.326	29.65 ± 0.973	472.1[a]
p_6 (nm)	62.29 ± 0.063	61.42 ± 0.077	57.8
σ_t (nm)	…	3.19 ± 0.060	…

[a]This value corresponds to the total grating height, i.e., $p_3 + p_5$.

TABLE II. Parameter correlation coefficient matrix.

	p_1	p_2	p_3	p_4	p_5	p_6	σ_t
p_1	1						
p_2	0.898	1					
p_3	−0.041	−0.186	1				
p_4	0.071	0.192	−0.991	1			
p_5	0.051	0.228	−0.994	0.977	1		
p_6	0.218	0.124	−0.521	0.603	0.440	1	
σ_t	−0.074	−0.056	0.247	−0.237	−0.241	−0.138	1

thus demonstrated that residual layer thickness nonuniformity is an important factor that induces the depolarization effects in characterizing nanoimprinted gratings.

Figure 2 shows the fitting result of the measured and calculated Mueller matrix spectra when incorporating the depolarization effects induced by numerical aperture, finite bandwidth, and residual layer thickness nonuniformity into the optical model. An excellent agreement can be observed from Fig. 2, which yields a fitting error of $\chi_r^2 = 25.22$. We also calculated the fitting error between the measured Mueller matrix spectra and the best-fit calculated Mueller matrix spectra obtained without considering any depolarization effect and achieved the value of $\chi_r^2 = 40.42$. Clearly, the depolarization effects exhibit a noticeable influence on the characterization of nanoimprinted gratings. It is also noted that the fit as shown in Fig. 2 does not have χ_r^2 close to 1. It might be because there are some unknown sources of depolarization that we did not take into account. In addition, the estimates of the standard deviations of the Mueller matrix elements provided by the RC2 ellipsometer may not reflect all of the errors in the measurement, since we found in our experiments that the estimates of the errors in the fitting parameters, obtained from the curvature of χ_r^2, underestimated the true errors. Table I presents the comparison of fitting parameters extracted from the MMP and SEM measurements. The uncertainties appended to the fitting parameter values that were extracted from MMP measurements all have a 95% confidence level. The fit1 in Table I shows the parameters extracted by MMP without considering any depolarization effect, whereas the fit2 shows the extracted parameters when taking the depolarization effects induced by numerical aperture, finite bandwidth, and residual layer thickness nonuniformity into account. As can be observed from Table I, fit2 is in excellent agreement with the results measured by SEM and has a much higher accuracy than fit1. It is also noted that the extracted structural parameters of the imprinted grating are in good agreement with the Si imprinting mold, which has a top critical dimension of 350 nm, a grating height of 472 nm, and a sidewall angle of 88°.[10] It therefore indicates an excellent fidelity of the nanoimprint pattern transfer process. Table II presents the parameter correlation coefficient matrix. The values of the parameter correlation coefficients fall between −1 and 1, with 0 meaning no correlation and with −1 and 1 meaning perfect correlation. It is noted from Table II that the correlation between the standard deviation σ_t of the residual layer thickness and other structural parameters is rather low, which demonstrates the decorrelation of σ_t from other parameters.

In summary, we have applied MMP to characterize nanoimprinted grating structures, and noticeable depolarization effects have been observed from the measured data. We have demonstrated that after incorporating the depolarization effects into the optical model, not only improved accuracy can be achieved for the line width, line height, and residual layer thickness measurement but also the residual layer thickness variation over the illumination spot can be directly determined by MMP.

This work was funded by the National Natural Science Foundation of China (Grant Nos. 91023032, 51005091, and 51121002) and the National Instrument Development Specific Project of China (Grant No. 2011YQ160002). The authors would like to thank Dr. Zhimou Xu and Mr. Tangyou Sun for preparing the nanoimprinted grating samples.

[1]S. Y. Chou, P. R. Krauss, and P. J. Renstrom, Science **272**, 85 (1996).
[2]S. Y. Chou, P. R. Krauss, W. Zhang, L. Guo, and L. Zhuang, J. Vac. Sci. Technol. B **15**, 2897 (1997).
[3]H.-J. Lee, C. L. Soles, H. W. Ro, R. L. Jones, E. K. Lin, W. Wu, and D. R. Hines, Appl. Phys. Lett. **87**, 263111 (2005).
[4]R. L. Jones, T. Hu, C. L. Soles, E. K. Lin, R. M. Reano, S. W. Pang, and D. M. Casa, Nano Lett. **6**, 1723 (2006).
[5]D. Fuard, C. Perret, V. Farys, C. Gourgon, and P. Schiavone, J. Vac. Sci. Technol. B **23**, 3069 (2005).
[6]R. M. Al-Assaad, S. Regonda, L. Tao, S. W. Pang, and W. Hu, J. Vac. Sci. Technol. B **25**, 2396 (2007).
[7]H. J. Patrick, T. A. Germer, Y. Ding, H. W. Ro, L. J. Richter, and C. L. Soles, Appl. Phys. Lett. **93**, 233105 (2008).
[8]T. Novikova, A. De Martino, S. B. Hatit, and B. Drévillon, Appl. Opt. **45**, 3688 (2006).
[9]M. Foldyna, A. De Martino, E. Garcia-Caurel, R. Ossikovski, C. Licitra, F. Bertin, K. Postava, and B. Drévillon, Eur. Phys. J.: Appl. Phys. **42**, 351 (2008).
[10]X. G. Chen, S. Y. Liu, C. W. Zhang, and H. Jiang, J. Micro/Nanolith. MEMS MOEMS **12**, 033013 (2013).
[11]G. E. Jellison, Jr. and J. W. McCamy, Appl. Phys. Lett. **61**, 512 (1992).
[12]U. Richter, Thin Solid Films **313–314**, 102 (1998).
[13]J. Li, J. J. Hwu, Y. Liu, S. Rabello, Z. Liu, and J. Hu, J. Micro/Nanolith. MEMS MOEMS **9**, 041305 (2010).
[14]M. G. Moharam, E. B. Grann, D. A. Pommet, and T. K. Gaylord, J. Opt. Soc. Am. A **12**, 1068 (1995).
[15]L. Li, J. Opt. Soc. Am. A **13**, 1870 (1996).
[16]S. Y. Liu, Y. Ma, X. G. Chen, and C. W. Zhang, Opt. Eng. **51**, 081504 (2012).
[17]R. W. Collins and J. Koh, J. Opt. Soc. Am. A **16**, 1997 (1999).
[18]J. J. Gil and E. Bernabeu, Opt. Acta **33**, 185 (1986).
[19]H. Fujiwara, *Spectroscopic Ellipsometry: Principles and Applications* (Wiley, New York, 2007).
[20]H. C. van de Hulst, *Light Scattering by Small Particles* (Wiley, New York, 1957).
[21]T. A. Germer and H. J. Patrick, Proc. SPIE **7638**, 76381F (2010).
[22]W. H. Press, S. A. Teukolsky, W. T. Vetterling, and B. P. Flannery, *Numerical Recipes: The Art of Scientific Computing*, 3rd ed. (Cambridge University Press, Cambridge, 2007).
[23]C. H. Herzinger, B. Johs, W. A. McGahan, J. A. Woollam, and W. Paulson, J. Appl. Phys. **83**, 3323 (1998).
[24]A. R. Forouhi and I. Bloomer, Phys. Rev. B **38**, 1865 (1988).